Letter

Anisotropic spin-to-charge conversion in bismuth

Hsia-Ling Liang,[1,*] T. C. Chuang,[1,*] Danru Qu,[2,3] C. C. Chiang,[1] Ming-Hao Lee,[2,3] Y. S. Chen,[2,3] Jauyn Grace Lin,[2,3] Ming-Wen Chu,[2,3] C. L. Chien,[1,4] and Ssu-Yen Huang[1,3,†]

[1]*Department of Physics, National Taiwan University, Taipei 10617, Taiwan*

[2]*Center for Condensed Matter Sciences, National Taiwan University, Taipei 10617, Taiwan*

[3]*Center of Atomic Initiatives for New Materials, National Taiwan University, Taipei 10617, Taiwan*

[4]*William H. Miller III Department of Physics and Astronomy, Johns Hopkins University, Baltimore, Maryland 21218, USA*

(Received 29 July 2021; revised 8 September 2022; accepted 2 November 2022; published 17 November 2022)

Many intriguing physical phenomena have emerged from the Bi-containing materials due to the interplay of band topology and strong spin-orbit coupling (SOC). In this work, we report anisotropic spin-to-charge conversion in Bi, a semimetal endowed with highly anisotropic Fermi surfaces in addition to strong SOC. The value of spin Hall angle θ_{SH} in Bi, that measures the spin-to-charge conversion efficiency, varies from $\theta_{SH} \approx 0$ to $\theta_{SH} \approx 2.6\%$ for two predominant crystal orientations. In addition, the propensity of oxidation and interface quality also affect the spin-to-charge conversion in Bi. The highly anisotropic spin-to-charge conversion between Bi(003) and Bi(012) provide significant insights into the exploration and development of Bi-based topological quantum materials and spintronics.

DOI: 10.1103/PhysRevB.106.L201304

Recently, pure spin current phenomena have attracted a great deal of attention. A pure spin current carries a spin angular momentum with a minimum of charge carriers, generates no Oersted field, and delivers spin-orbit torque that can efficiently switch ferromagnetic entities. Spin Hall effect (SHE), spin Seebeck effect (SSE), and spin pumping (SP) are the main mechanisms for generating a pure spin current $\boldsymbol{J}_S$. A heavy metal (HM) with strong spin-orbit coupling (SOC) can indirectly detect $\boldsymbol{J}_S$ via the inverse spin Hall effect (ISHE) in a HM by converting it into a charge current $\boldsymbol{J}_C$ according to

$$J_C = (2e/\hbar)\theta_{SH} J_S \times \sigma \tag{1}$$

and often detected as an ISHE voltage, where $\hbar$ is the reduced Planck constant, e the electronic charge, $\boldsymbol{\sigma}$ the spin index, and θ_{SH} is the spin Hall angle that specifies the conversion efficiency. Both charge transport and spin transport in metals, dominated by electrons at the Fermi energy of the Fermi surface, depend on the topology and geometry of band structures. Among the contributions of the SHE, the intrinsic Berry curvature contribution would reflect the anisotropic Fermi surfaces.

Pure spin current phenomena have been extensively explored mostly in HMs with cubic symmetry (e.g., Pt, Ta, and W), for which all directions exhibit strong spin-to-charge conversion with little (e.g., less than 20% in Pt layers of different orientations) or no anisotropy [1–3]. But for noncubic materials, e.g., hexagonal and tetragonal materials, the magnitude could be highly anisotropic and even the sign of the spin Hall conductivity could change [1]. Therefore, anisotropic spin-to-charge conversion can best be explored in HMs with strong SOC and with highly anisotropic Fermi surfaces, such as bismuth (Bi). Being the heaviest nonradioactive element in the Periodic Table, Bi not only has the interaction of band topology and strong spin-orbit coupling but is also endowed with one of the most highly anisotropic Fermi surfaces, consisting of elongated ellipsoidal surfaces for both electrons and holes [4]. As a result, highly anisotropic properties in resistance, magnetoresistance, and Shubnikov–de Haas oscillations, have been observed in Bi [4,5]. However, the pure spin current phenomena in Bi have been complicated in part due to its pronounced ordinary Nernst effect (ONE), which interferes with the measurement of the ISHE voltage. This may have contributed to the large variances of the spin Hall angle θ_{SH} by as much as three orders of magnitude in Bi thin films [6–12]. Considering the crucial role of Bi in quantum materials and potential spintronic applications, it is important to explore the anisotropy of spin-to-charge conversions in Bi.

We report in this work a highly anisotropic spin-to-charge conversion in Bi layers of two predominant orientations, the most anisotropic reported to date. We show that the value of θ_{SH} in Bi varies from negligible to significant for different crystalline orientations of the Bi thin layers. In addition, we demonstrate that the spin-to-charge conversion in Bi is strongly influenced by the quality of the interface and the degree of oxidation, which has been overlooked in some works. Our results offer the criteria for generating and detecting spin current in Bi by electrical means, providing insight into the exploration and development of Bi-based topological quantum and spintronic materials.

Bismuth has a rhombohedral crystal structure, often described using a hexagonal system with the trigonal axis as the c axis. The most common orientation of Bi thin films made

*H.-L. Liang and T. C. Chuang contributed equally to this work.
†syhuang@phys.ntu.edu.tw

by sputtering, evaporation, and molecular beam epitaxy is the c-axis film known as Bi(111) in rhombohedral or Bi(003) in hexagonal notation. In the following, we use exclusively the hexagonal notation, where the c axis is normal to the Bi(003) plane. After exploring the sputtering parameters, we have also found that Bi thin films on $Y_3Fe_5O_{12}$ (YIG) with exclusive Bi(003) or Bi(012) texture can be accomplished using sputtering at room temperature under the following conditions:

(1) Bi(003)/YIG: dc sputtering at voltage = 260 V, current = 80 mA, or power = 20 W.

(2) Bi(012)/YIG: rf sputtering at bias voltage = 64 V, power = 20 W.

These Bi thin films are then capped *in situ* with a 3-nm layer of SiO_2, except when addressing the potential oxidation problem. The thickness and surface roughness of Bi and YIG films are measured by x-ray reflectometry and atomic force microscopy, respectively. The surface roughness of YIG and the 15-nm-thick Bi on YIG are about 0.5 and 2 nm, respectively. The thin-film crystal structures and orientations are determined by x-ray diffraction (XRD) and transmission electron microscopy. The cross-sectional high-angle annular dark-field (HAADF) imaging by scanning transmission electron microscopy (STEM) was conducted on a spherical-aberration corrected microscope, JEOL 2100FX, at 200 kV. The electron probe size is of ∼1 Å and the HAADF-imaging collection angle is of 70–190 mrad. The specimen was prepared by focused ion beam. We use a vibrating sample magnetometer to measure the magnetic properties of the materials.

We employ longitudinal spin Seebeck effect [13,14] and spin pumping [15,16], the two established pure spin current injection schemes to study the spin-to-charge conversions in Bi. To eliminate the parasitic effects from electric charge contributions, we refrain from using ferromagnetic metals such as permalloy [17]. Instead, we use only ferrimagnetic insulator YIG to inject a pure spin current by a temperature gradient in longitudinal spin Seebeck effect (LSSE) or microwave excitations in SP. In Bi/YIG, the injected pure spin current $\boldsymbol{J}_S$ into Bi is then detected by the ISHE. Only voltages that adhere to Eq. (1) can be attributed to $\boldsymbol{J}_S$.

We first describe the ISHE voltage in the Bi(003) films from the LSSE. To generate a pure spin current by the SSE, we employ a longitudinal experimental setup with a resistive heater and a Cu heat sink, on the top and the bottom of the sample, respectively. This ensures a uniform out-of-plane temperature and the same heat flux for each measurement. The temperature difference is measured with thermocouples. We use bulk YIG slabs and YIG thin films to inject pure spin currents into the Bi layers. The poly-YIG and epi-YIG denote polycrystalline and epitaxial YIG films, respectively, and the YIG slab denotes the bulk YIG slab. As illustrated in Fig. 1(a), an out-of-plane temperature gradient $\nabla \boldsymbol{T}$ in the z direction injects a spin current $\boldsymbol{J}_S$ from YIG into the Bi layer, with the spin orientation $\boldsymbol{\sigma}$ in the x direction as aligned by an external magnetic field $\boldsymbol{H}$. The charge current $\boldsymbol{J}_C$ is subsequently converted from $\boldsymbol{J}_S$ via the ISHE in the Bi layer according to Eq. (1). As such, the ISHE voltage due to $\boldsymbol{J}_C$ must display the field dependence of $\boldsymbol{\sigma}$, that of the magnetization $\boldsymbol{M}$ of YIG. In particular, at sufficiently large fields, $\boldsymbol{M}$, $\boldsymbol{J}_C$, and hence the ISHE voltage must saturate. For Bi(003)/YIG, the measured voltage instead is linearly proportional to the magnetic field without saturation, as shown in Fig. 1(b). This is not the ISHE voltage, but the linear thermal voltage caused by the ONE, the thermal analog of the ordinary Hall effect. Indeed, Bi has the largest ONE effect of all elements, hence a very pronounced voltage but unrelated to spin current. There is no detectable voltage that saturates with $\boldsymbol{M}$ of YIG due to spin current, hence $\theta_{SH} \approx 0$. This result agrees with the previously reported negligible spin-to-charge conversion in Bi by the LSSE and SP measurements [9,10].

In sharp contrast, the spin-to-charge conversion is sizable in the Bi(012) films. As shown in Fig. 1(c), in addition to the voltage linear in field due to the ONE, there is a large ISHE voltage that saturates when the magnetization of YIG is aligned by $\boldsymbol{H}$. Moreover, the ISHE signal of the Bi(012) films remains robust using different pure spin current injectors, including poly-YIG, epi-YIG, and polycrystalline YIG slab. The robust and consistent ISHE voltages indicate similar interface spin current transparency among different Bi(012)/YIGs samples for the SSE measurement, while the hysteresis loops of the Bi ISHE voltages reflect different YIG materials. The coercivity of poly-YIG films is about 20 Oe, which is 15 Oe larger than that for the epi-YIG [13]. The hysteresis loop of the YIG slab is wider with a plateau in the low field region due to the surface magnetization from the demagnetizing field, as previously shown [14]. While the loop behavior of the ISHE voltages depends on different YIGs, the background voltage linear in the field for all samples is due to the large intrinsic ONE in Bi, unrelated to pure spin current. After the insertion of a 5-nm SiO_2 layer between Bi(012) and YIG, the ISHE voltage vanishes, and only the ONE voltage remains, as shown in Fig. 1(d).

We further utilize SP to confirm the spin-to-charge conversion in the 15-nm-thick Bi(012) films. As shown in Fig. 2(a), the SP experiment is conducted at room temperature using a TE102 cavity with a microwave power of 100 mW at a frequency of 9.77 GHz. When YIG is in a ferromagnetic resonance (FMR) state at the resonance field (H_R), as shown by the derivatives of the FMR spectra in Figs. 2(b) and 2(c), the SP-induced ISHE voltage for the Bi(012) films on poly-YIG and epi-YIG can be detected. While the LSSE-induced ISHE is insensitive to poly-YIG and epi-YIG, as shown in Fig. 1(c), the SP-generated ISHE voltage from epi-YIG films exhibits a much sharper linewidth and more prominent signal, 50 times larger than that of the poly-YIG films. These results reveal the key difference between the two injection mechanisms: SP relies on collective motions of magnetic moments driven by FMR, whereas LSSE is due to incoherently excited magnons with a long magnon diffusion length [13]. Therefore, a higher degree of crystallinity and homogeneity results in a stronger SP signal. In the study of the SP-induced ISHE voltage for Bi(003) thin layers, the signal is negligible as was concluded from the LSSE experiment (see Supplemental Material [18]). Furthermore, after inserting a 5-nm SiO_2 layer that blocks the spin current, the ISHE from SP becomes negligible, affirming that it is a spin current effect.

Both LSSE and SP measurements confirm the positive and large spin-to-charge conversion in the Bi(012) layer but negligible in the Bi(003) layer. Next, we ascertain that these contrasting behaviors are intrinsic to Bi and not related to

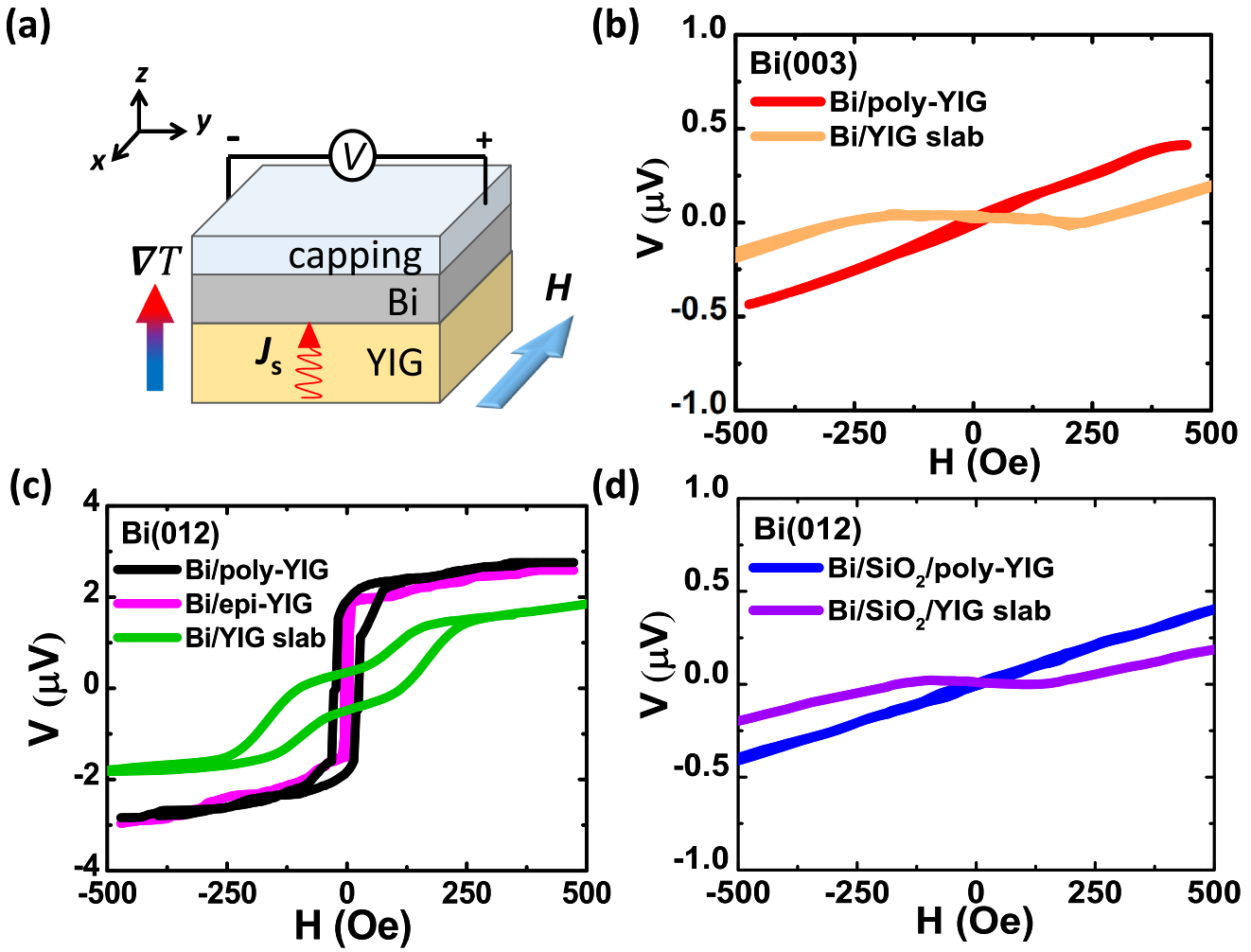

FIG. 1. Longitudinal spin Seebeck effect (LSSE). (a) Schematic of LSSE in Bi(15 nm)/YIG systems. The inverse spin Hall effect signals as a function of magnetic field (H) are measured in (b) Bi(003) on poly-YIG and YIG slab, (c) Bi(012) on poly-YIG, epi-YIG, and YIG slab, and (d) with a spin current-blocking SiO_2 layer inserted between Bi(012) and poly-YIG and YIG slab. All data contain a voltage linear in H due to the ordinary Nernst effect of Bi.

the layer quality. The XRD patterns disclose that both layers have the hexagonal structure with the Bi(003) and the Bi(012) orientations, as shown in Figs. 3(a) and 3(c), where Bi(003) and Bi(012) are the dominating structures, respectively. The STEM-HAADF imaging reveals well-oriented lattices with structural sharpness across the interface between Bi and YIG for both Bi(012)/YIG and Bi(003)/YIG as shown in Figs. 3(b) and 3(d), respectively. The fast Fourier transforms [insets in Figs. 3(b) and 3(d); equivalent to electron diffraction] of the Bi films and YIG substrates unveil the characteristic crystallographic orientations. The Bi(012) and the Bi(003) vectors are parallel to the YIG(420) in Figs. 3(b) and 3(d), respectively, corroborating the XRD patterns in Figs. 3(a) and 3(c). The lattice schemes of the Bi and YIG are also superimposed with the atomistic contrasts of cations directly imaged in Figs. 3(b) and 3(d) and the agreements indicate an unambiguous crystallinity of the materials. These findings affirm the quality of our Bi/YIG. Note that the 3-nm SiO_2 protective layer is essential for the sample integrity. In contrast, for the bare Bi layer without the SiO_2 layer, the sharpness of the crystalline structure no longer exists, and the ISHE voltage deteriorates with time due to oxidation in Bi (see Supplemental Material [18]).

To quantitatively determine the spin Hall angle θ_{SH} and spin-diffusion length λ_{sf}, we conduct thickness-dependent studies through the LSSE. Figure 4(a) shows the representative results for Bi(012). The magnitude of the ISHE signal varies strongly with Bi thickness due to the decaying of the spin current. These samples have been individually fabricated, and their ISHE voltages all have a similar coercivity (∼20 Oe), highlighting the consistency among different samples. As detailed elsewhere, the ISHE voltage $V_{ISHE}(t)$ varies with thickness t as [19]

$$\frac{V(t)}{\rho(t)L\nabla T} = 2C\theta_{SH}\frac{\lambda_{sf}}{t}\tanh\left(\frac{t}{2\lambda_{sf}}\right), \tag{2}$$

where $L = 5$ mm is the sample length, and $\nabla T = 14$ K/mm is the temperature gradient, measured by typical thermocouples and normalized by the sample thickness. $C =$

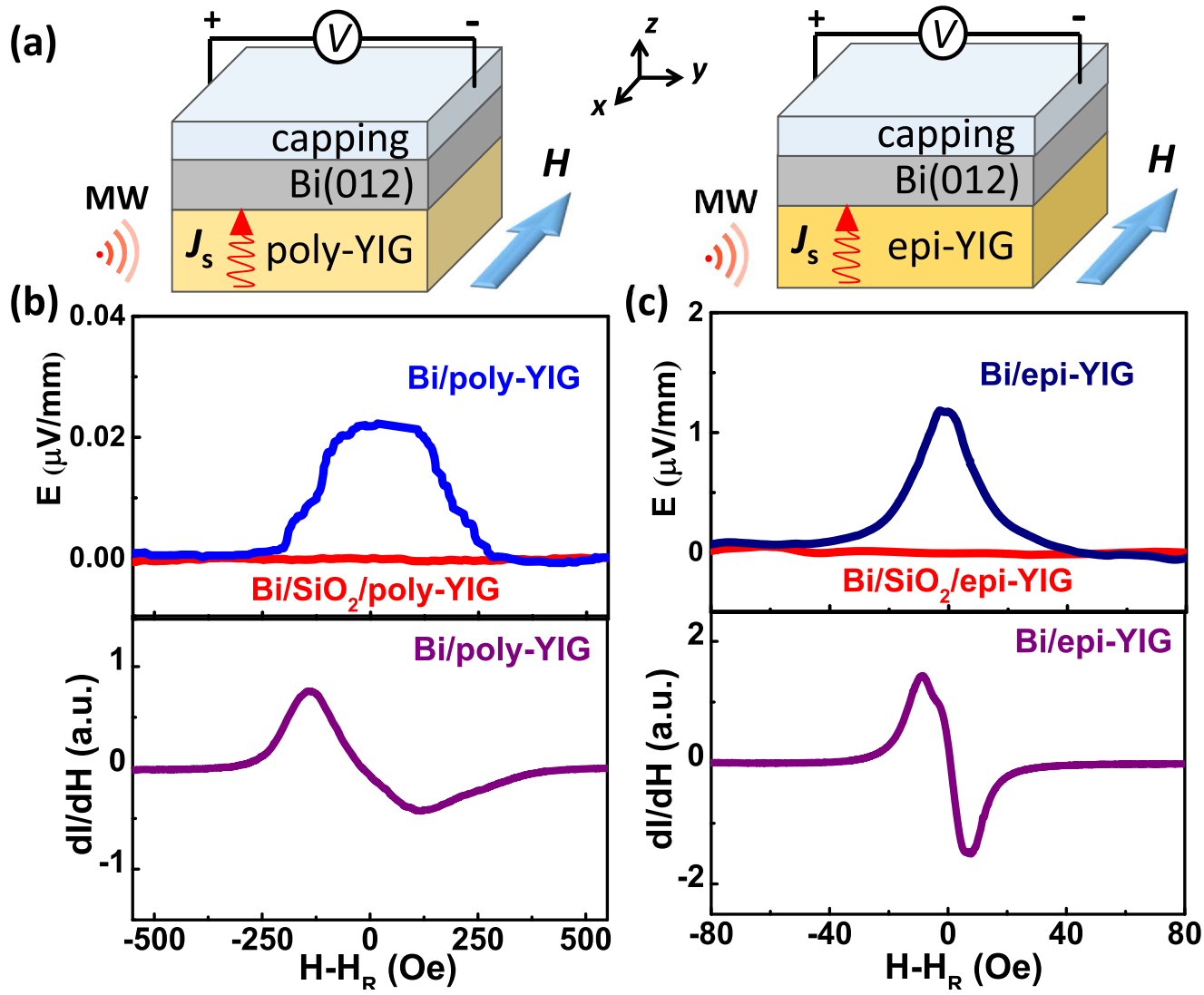

FIG. 2. Spin pumping. Schematic of spin pumping in (a) Bi(012)/poly-YIG and Bi(012)/epi-YIG systems. The ISHE signals as a function of magnetic field (H) subtracting the resonance field (H_R) and microwave absorption spectrum in (b) Bi(012)/poly-YIG and (c) Bi(012)/epi-YIG systems. The ISHE signals vanish with the insertion of the SiO_2 layer that blocks the spin current. The thickness of Bi is 15 nm and the microwave frequency is 9.77 GHz.

$\frac{2e}{\hbar}\frac{\gamma\hbar\rho' k_m^3 l_m}{4\pi M\pi^2}\frac{B_1 B_s}{B_2} g_{\rm eff}^{\uparrow\downarrow} k_{\rm B}$ is the spin current injection coefficient [16], which contains the magnetic properties of YIG (saturation magnetization $4\pi M = 1500$ Oe, gyromagnetic ratio $\gamma = 1.48 \times 10^{11}$ s^{-1} T^{-1}, magnon diffusion length $l_{\rm m} = 70$ nm, finite ferromagnetic insulator thickness factor $\rho' \sim 1$, maximum wave number $k_{\rm m} = 2 \times 10^9$ m^{-1}, parameters from the diffusion equation $B_1 = 0.55$, $B_{\rm s} = 2.2 \times 10^{-4}$, $B_2 = 5.1 \times 10^{-3}$) [20], the electron charge $e = 1.6 \times 10^{-19}$ C, the Boltzmann constant $k_{\rm B} = 1.38 \times 10^{-23}$ J K^{-1}, the reduced Planck constant $\hbar = 1.054 \times 10^{-34}$ J s, and $g_{\rm eff}^{\uparrow\downarrow} = 1.3 \times 10^{18}$ m^{-2} is the spin mixing conductance between the Bi and YIG layer [9]. Among all the factors, the resistivity $\rho(t)$ has the strongest variation in thin films and must be measured. The results of the resistivity of the samples of Bi(012)/YIG are shown in the inset of Fig. 4(b). As expected, the resistivity of the Bi thin films is constant at large thicknesses but increases with decreasing film thickness at small thickness due to the surface and boundary scattering, which is well described by the Fuchs-Sondheimer theory [21], $\rho = \rho_{\rm bulk}[1 + (\frac{3\updownarrow}{8t})(1-p)]$ with bulk resistivity $\rho_{\rm bulk}$, electron mean free path $\updownarrow$, and specular scattering p. From the best-fit result, $\rho_{\rm bulk}$ is determined to be 105 $\mu\Omega$ cm with a relatively long $\ell \sim 250$ nm, consistent with the semimetal properties of Bi with small effective carrier mass and large Fermi wavelength. Note that the ISHE voltages drop sharply below 15 nm, as shown in Fig. 4(b), due to the combination of several effects, including spin backflow [22], where spins diffuse back into the ferromagnet before converting to charge, and the loss of spin information caused by the enhanced surface scatterings. Thus, data from these very thin films are excluded in our analysis. From the fitting in Fig. 4(b), we obtain $\theta_{\rm SH} = 2.6 \pm 0.8\%$ and $\lambda_{\rm sf} = 5.76 \pm 2.6$ nm in Bi(012). This large value of $\theta_{\rm SH} = 2.6\%$ in Bi(012) is comparable to those of heavy metals (e.g., Pt) with the largest $\theta_{\rm SH}$, whereas in contrast, $\theta_{\rm SH} \approx 0$ in Bi(003).

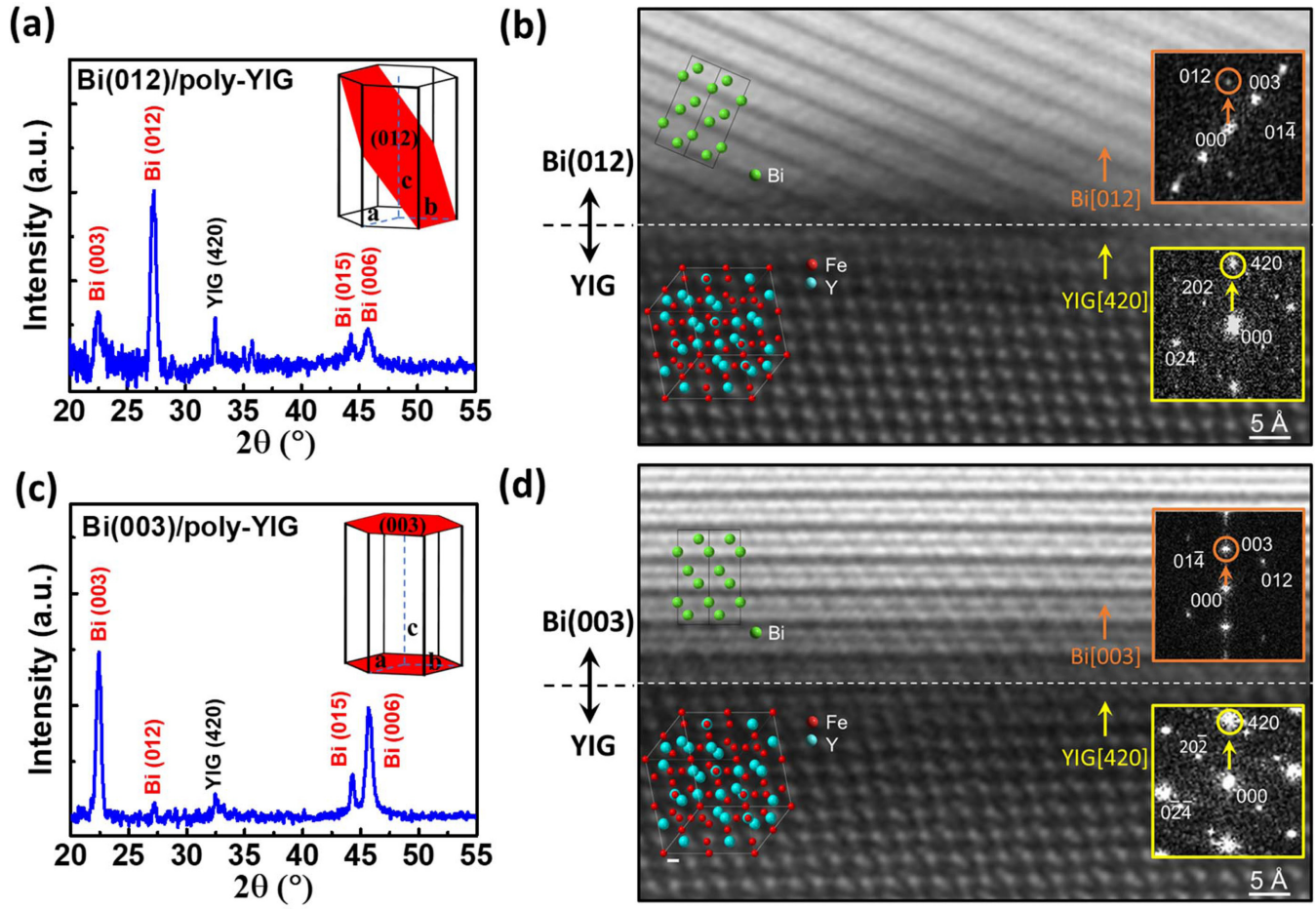

FIG. 3. XRD patterns and STEM-HAADF imaging. The XRD patterns of (a) Bi(012)/poly-YIG and (c) Bi(003)/poly-YIG with the preferred crystal planes highlighted by red in the hexagonal crystal structure. The STEM-HAADF imaging of the (b) Bi(012)/poly-YIG and (d) Bi(003)/poly-YIG bilayers, revealing a structural sharpness across the interfaces. Insets in (b) and (d): Fast Fourier transforms of the respective Bi films (orange-framed) and YIG films (yellow-framed) indicating the characteristic crystallographic orientations.

This is the largest contrast in pure spin current phenomena reported to date. Throughout our analysis, we consider λ_{sf} as a constant value, since films with comparable resistivity are investigated. While for a more careful study, λ_{sf} could reduce when thickness decreases due to the enhanced Elliot-Yafet scattering [23], resulting in an even larger θ_{SH}.

In addition to the ISHE, another possible mechanism that has been suggested for the spin-to-charge conversion in Bi is the inverse Rashba-Edelstein effect (IREE), which is attributed to Rashba splitting at the interface [24,25]. The IREE associated with the interfacial Rashba effect of Bi is expected to be independent of its thickness, whereas the ISHE due to bulk SOC of Bi is thickness dependent due to the short spin-diffusion length [9]. From the thickness-dependent results, we conclude that the spin conversion in Bi/YIG is attributed to the ISHE. This is further corroborated by the temperature-dependent behavior. We compare the results of Bi/YIG with those of Pt(5 nm)/YIG with bulk ISHE of Pt. As shown in Fig. 4(c), while the temperature (T) dependent resistivity $\rho(T)$ of heavy metal Pt decreases with decreasing temperature, that of semimetal Bi shows the opposite trend. In contrast, the spin-to-charge conversion, represented by the ISHE voltage $V(T)$ normalized by $\rho(T)$, for both Pt/YIG and Bi/YIG, exhibit the similar temperature dependence as shown in Fig. 4(d). The temperature dependence of magnon population and magnon propagation length in YIG gives rise to this temperature-dependent nonmonotonic behavior [26,27]. This observation confirms the bulk origin of the ISHE effect in Bi. An SP experiment has also concluded ISHE rather than IREE in Bi [28].

Although Bi with strong spin-orbit coupling has been a pivotal element for topological quantum materials [29–36], with notable examples in three-dimensional topological insulators (e.g., Bi_2Se_3 and $Bi_{1-x}Sb_x$ alloy [32–35]) and topological superconductors (e.g., $\beta-Bi_2Pd$ [36,37]), pure Bi has been concluded by most studies to be topologically trivial. However, recent theoretical studies and experimental results, including high-resolution angle-resolved photoemission spectroscopy measurements, reveal the band structure in pure Bi may be topologically nontrivial, which could lead to a large Berry curvature [38–41]. It is also demonstrated that the surface state of Bi is strongly spin-orbit split with electron spin-momentum locking [42–45]. Moreover, it has been reported that when using two different definitions of the spin current, the flow of spin angular momentum and the flow of the spin magnetic moment, to calculate the spin Hall conductivity of the Dirac material Bi, completely different results are achieved [46]. The highly anisotropic spin-to-charge

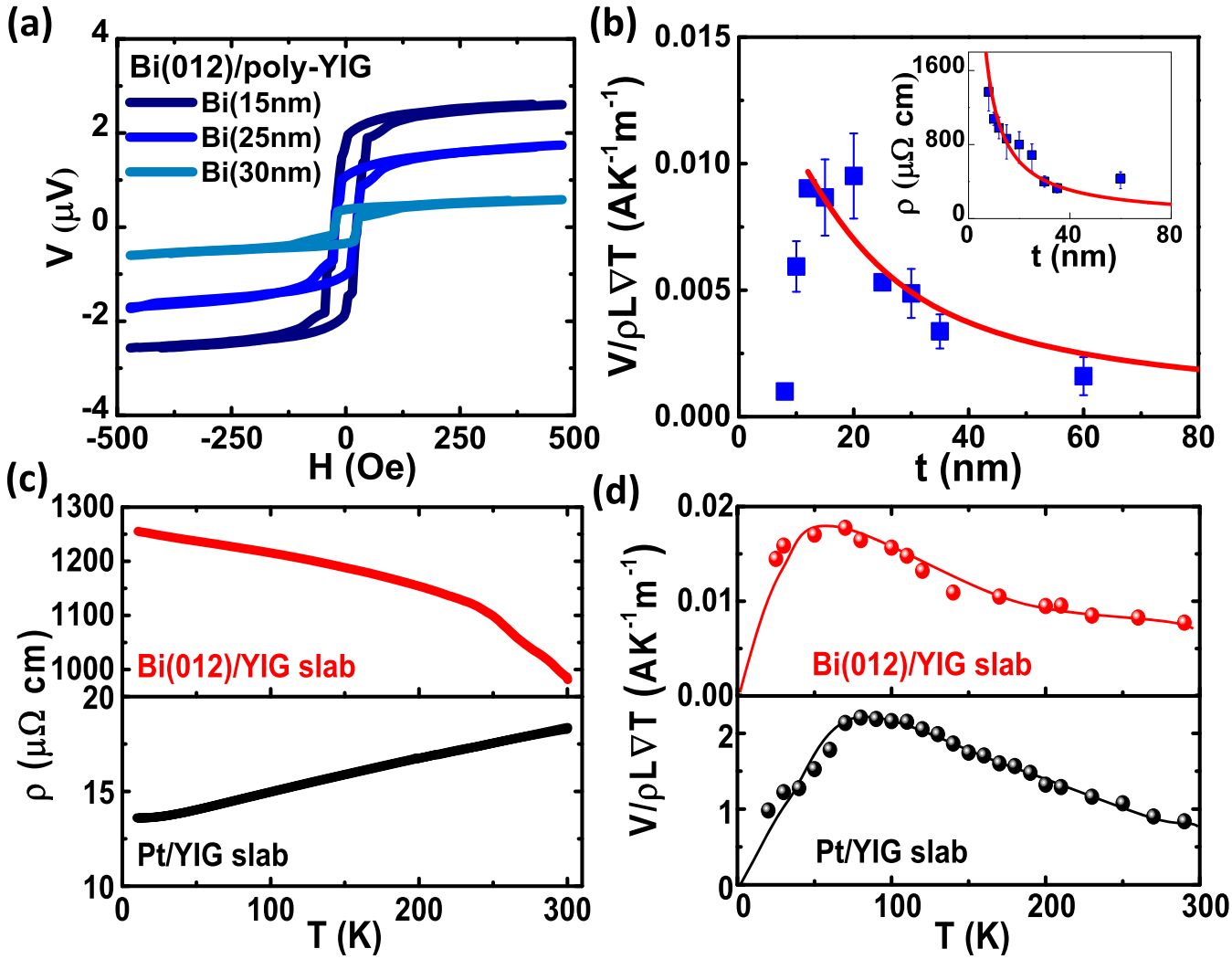

FIG. 4. Thickness dependence. (a) LSSE measurement in Bi(012)/poly-YIG samples with different thicknesses of Bi layer. (b) Thickness-dependent normalized ISHE signal fitted by spin transport model. The inset displays the thickness-dependent electrical resistivity fitted by the Fuchs-Sondheimer model. (c) The temperature-dependent resistivity for Bi(012)/YIG slab and Pt/YIG slab. (d) The temperature-dependent normalized ISHE signals in Bi(012)/YIG slab and Pt/YIG slab. The solid lines are guides to the eyes.

conversion in Bi uncovered in our study could correlate with the anisotropic SOC and the topological nature of Bi but awaits rigorous theoretical calculations.

Bismuth is an important and intriguing element for many quantum materials. In this work, we show that the hexagonal crystal structure of Bi with highly anisotropic SOC and Fermi surfaces profoundly modifies the spin-to-charge conversion in Bi of different orientations. To quantitatively determine the spin Hall angle, we conduct a self-consistent method by thermally injecting spin current from YIG into Bi with different thicknesses and performing spin current analyses. Our results show $\theta_{SH} \approx 2.6\%$ for Bi(012), but $\theta_{SH} \approx 0$ for Bi(003), revealing highly anisotropic spin-to-charge conversion, the largest contrast to date, which still awaits rigorous theoretical studies. Through atomic-level structural analysis using high-resolution STEM imaging, we further reveal that for consistent and robust spin conversion in Bi, the protection of Bi from oxidation is essential. Our results address the experimental criteria for the spin conversion in Bi, which is important for Bi-based topological quantum materials and spintronics.

Note added. Recently, we noticed that a preprint [47] uses ST-FMR and shows gigantic anisotropic spin conversion between the rhombohedral Bi(111) and Bi(110), which is consistent with the results reported in this Letter.

The authors would like to thank T. Y. Chen for XRD measurements. We acknowledge very helpful discussions with G. Y. Guo. This work was supported by the Ministry of Science and Technology of Taiwan under Grants No. MOST 109-2123-M-002-002 and No. 110-2123-M-002-008. This study was also partially supported by Center of Atomic Initiative for New Materials from the Featured Areas Research Center Program within the framework of the Higher Education Sprout Project by the Ministry of Education in Taiwan.

[1] F. Freimuth, S. Blügel, and Y. Mokrousov, Anisotropic Spin Hall Effect from First Principles, Phys. Rev. Lett. **105**, 246602 (2010).

[2] C. Guillemard, S. Petit-Watelot, S. Andrieu, and J. C. Rojas-Sánchez, Charge-spin current conversion in high quality epitaxial Fe/Pt systems: Isotropic spin Hall angle along different in-plane crystalline directions, Appl. Phys. Lett. **113**, 262404 (2018).

[3] R. Thompson, J. Ryu, G. Choi, S. Karube, M. Kohda, J. Nitta, and Byong-Guk Park, Anisotropic Spin-Orbit Torque through Crystal-Orientation Engineering in Epitaxial Pt, Phys. Rev. Appl. **15**, 014055 (2021).

[4] V. S. Édel'man, Electrons in bismuth, Adv. Phys. **25**, 555 (1976).

[5] F. Y. Yang, K. Liu, K. Hong, D. H. Reich, P. C. Searson, C. L. Chien, Y. Leprince-Wang, Kui Yu-Zhang, and K. Han, Shubnikov–de Haas oscillations in electrodeposited single-crystal bismuth films, Phys. Rev. B **61**, 6631 (2000).

[6] D. Hou, Z. Qiu, K. Harii, Y. Kajiwara, K. Uchida, Y. Fujikawa, H. Nakayama, T. Yoshino, T. An, K. Ando, X. Jin, and E. Saitoh, Interface induced inverse spin Hall effect in bismuth/permalloy bilayer, Appl. Phys. Lett. **101**, 042403 (2012).

[7] H. Emoto, Y. Ando, E. Shikoh, Y. Fuseya, T. Shinjo, and M. Shiraishi, Conversion of pure spin current to charge current in amorphous bismuth, J. Appl. Phys. **115**, 17C507 (2014).

[8] S. Sangiao, J. M. De Teresa, L. Morellon, I. Lucas, M. C. Martinez-Velarte, and M. Viret, Control of the spin to charge conversion using the inverse Rashba-Edelstein effect, Appl. Phys. Lett. **106**, 172403 (2015).

[9] H. Emoto, Y. Ando, G. Eguchi, R. Ohshima, E. Shikoh, Y. Fuseya, T. Shinjo, and M. Shiraishi, Transport and spin conversion of multicarriers in semimetal bismuth, Phys. Rev. B **93**, 174428 (2016).

[10] D. Yue, W. Lin, J. Li, X. Jin, and C. L. Chien, Spin-to-Charge Conversion in Bi Films and Bi/Ag Bilayers, Phys. Rev. Lett. **121**, 037201 (2018).

[11] M. Matsushima, S. Miwa, S. Sakamoto, T. Shinjo, R. Ohshima, Y. Ando, Y. Fuseya, and M. Shiraishi, Sizable spin-transfer torque in the $Bi/Ni_{80}Fe_{20}$ bilayer film, Appl. Phys. Lett. **117**, 042407 (2020).

[12] S. Sangiao, J. I. Morales-Aragonés, I. Lucas P. Jiménez-Cavero, L. Morellón, C. Sánchez-Azqueta, and J. M. D. Teresa, Optimization of YIG/Bi stacks for spin-to-charge conversion and influence of aging, J. Phys. D: Appl. Phys. **54**, 375305 (2021).

[13] F.-J. Chang, J. G. Lin, and S.-Y. Huang, Robust spin current generated by the spin Seebeck effect, Phys. Rev. Mater. **1**, 031401(R) (2017).

[14] P.-H. Wu and S.-Y. Huang, Noncollinear magnetization between surface and bulk Y_3Fe_5O, Phys. Rev. B **94**, 024405 (2016).

[15] H. L. Wang, C. H. Du, Y. Pu, R. Adur, P. C. Hammel, and F. Y. Yang, Scaling of Spin Hall Angle in 3d, 4d, and 5d Metals from Y_3Fe_5O/Metal Spin Pumping, Phys. Rev. Lett. **112**, 197201 (2014).

[16] Y. S. Chen, J. G. Lin, S. Y. Huang, and C. L. Chien, Incoherent spin pumping from YIG single crystals, Phys. Rev. B **99**, 220402(R) (2019).

[17] S. Y. Huang, D. Qu, T. C. Chuang, C. C. Chiang, W. Lin, and C. L. Chien, Pure spin current phenomena, Appl. Phys. Lett. **117**, 190501 (2020).

[18] See Supplemental Material at http://link.aps.org/supplemental/10.1103/PhysRevB.106.L201304 for effects of oxidation on ISHE in capped and uncapped Bi thin films, spin pumping measurement for Bi(003), and XRD patterns and magnetic measurement for the poly-YIG slab, poly-YIG film, and epi-YIG film.

[19] D. Qu, S. Y. Huang, B. F. Miao, S. X. Huang, and C. L. Chien, Self-consistent determination of spin Hall angles in selected 5d metals by thermal spin injection, Phys. Rev. B **89**, 140407(R) (2014).

[20] S. M. Rezende, R. L. Rodríguez-Suárez, R. O. Cunha, A. R. Rodrigues, F. L. A. Machado, G. A. Fonseca Guerra, J. C. Lopez Ortiz, and A. Azevedo, Magnon spin-current theory for the longitudinal spin-Seebeck effect, Phys. Rev. B **89**, 014416 (2014).

[21] T. C. Chuang, P. L. Su, P. H. Wu, and S. Y. Huang, Enhancement of the anomalous Nernst effect in ferromagnetic thin films, Phys. Rev. B **96**, 174406 (2017).

[22] H. J. Jiao and G. E. W. Bauer, Spin Backflow and ac Voltage Generation by Spin Pumping and the Inverse Spin Hall Effect, Phys. Rev. Lett. **110**, 217602 (2013).

[23] M.-H. Nguyen, D. C. Ralph, and R. A. Buhrman, Spin Torque Study of the Spin Hall Conductivity and Spin Diffusion Length in Platinum Thin Films with Varying Resistivity, Phys. Rev. Lett. **116**, 126601 (2016).

[24] J. C. Sánchez, L. Vila, G. Desfonds, S. Gambarelli, J. P. Attané, J. M. De Teresa, C. Magén, and A. Fert, Spin-to-charge conversion using Rashba coupling at the interface between non-magnetic materials, Nat. Commun. **4**, 2944 (2013).

[25] C. R. Ast, J. Henk, A. Ernst, L. Moreschini, M. C. Falub, D. Pacilé, P. Bruno, K. Kern, and M. Grioni, Giant Spin Splitting through Surface Alloying, Phys. Rev. Lett. **98**, 186807 (2007).

[26] E.-J. Guo, J. Cramer, A. Kehlberger, C. A. Ferguson, D. A. MacLaren, G. Jakob, and M. Kläui, Influence of Thickness and Interface on the Low-Temperature Enhancement of the Spin Seebeck Effect in YIG Films, Phys. Rev. X **6**, 031012 (2016).

[27] P.-H. Wu, Y. C. Tu, D. Qu, H.-L. Liang, S.-F. Lee, and S.-Y. Huang, Probing the spin-glass freezing transition in $Cu_{1-x}Mn_x$ alloy by spin current, Phys. Rev. B **101**, 104413 (2020).

[28] J. Shen, Z. Feng, P. Xu, D. Hou, Y. Gao, and X. Jin, Spin-to-Charge Conversion in Ag/Bi Bilayer Revisited, Phys. Rev. Lett. **126**, 197201 (2021).

[29] M. Z. Hasan and C. L. Kane, "Colloquium: Topological insulators," Rev. Mod. Phys. **82**, 3045 (2010).

[30] X.-L. Qi and S.-C. Zhang, "Topological insulators and superconductors," Rev. Mod. Phys. **83**, 1057 (2011).

[31] P. Liu, J. R. Williams, and J. J. Cha, Topological nanomaterials, Nat. Rev. Phys. **4**, 479 (2019).

[32] Xia, Y. D. Qian, D. Hsieh, L. Wray, A. Pal, H. Lin, A. Bansil, D. Grauer, Y. S. Hor, R. J. Cava, and M. Z. Hasan, Observation of a large-gap topological-insulator class with a single Dirac cone on the surface, Nat. Phys. **5**, 398 (2009).

[33] H. Zhang, C. X. Liu, X. L. Qi, X. Dai, Z. Fang, and S. C. Zhang, Topological insulators in Bi_2Se_3, Bi_2Te_3 and Sb_2Te_3 with a single Dirac cone on the surface, Nat. Phys. **5**, 438 (2009).

[34] J. C. Y. Teo, L. Fu, and C. L. Kane, Surface states and topological invariants in three-dimensional topological insulators: Application to $Bi_{1-x}Sb_x$, Phys. Rev. B **78**, 045426 (2008).

[35] D. Hsieh, D. Qian, L. Wray, Y. Xia, Y. S. Hor, R. J. Cava, and M. Z. Hasan, A topological Dirac insulator in a quantum spin Hall phase, Nature (London) **452**, 970 (2008).

[36] Y. Li, X. Xu, M.-H. Lee, M.-W. Chu, and C. L. Chien, Observation of half-quantum flux in the unconventional superconductor $\beta-Bi_2Pd$, Science **366**, 238 (2019).

[37] X. Xu, Y. Li, and C. L. Chien, Spin-Triplet Pairing State Evidenced by Half-Quantum Flux in a Noncentrosymmetric Superconductor, Phys. Rev. Lett. **124**, 167001 (2020).

[38] S. Ito, B. Feng, M. Arita, A. Takayama, R.-Y. Liu, T. Someya, W.-C. Chen, T. Iimori, H. Namatame, M. Taniguchi, C.-M. Cheng, S.-J. Tang, F. Komori, K. Kobayashi, T.-C. Chiang, and I. Matsuda, Proving Nontrivial Topology of Pure Bismuth by Quantum Confinement, Phys. Rev. Lett. **117**, 236402 (2016).

[39] F. Schindler, Z. Wang, M. G. Vergniory, A. M. Cook, A. Murani, S. Sengupta, A. Yu. Kasumov, R. Deblock, S. Jeon, I. Drozdov, H. Bouchiat, S. Guéron, A. Yazdani, B. A. Bernevig, and T. Neupert, Higher-order topology in bismuth, Nat. Phys. **14**, 918 (2018).

[40] T.-R. Chang, Q. Lu, X. Wang, H. Lin, T. Miller, T.-C. Chiang, and G. Bian, Band topology of bismuth quantum films, Crystals **9**, 510 (2019).

[41] C.-H. Hsua, X. Zhou, T.-R. Chang, Q. Ma, N. Gedik, A. Bansil, S.-Y. Xu, H. Lin, and L. Fu, Topology on a new facet of bismuth, Proc. Natl Acad. Sci. USA **116**, 13255 (2019).

[42] Yu. M. Koroteev, G. Bihlmayer, J. E. Gayone, E. V. Chulkov, S. Blügel, P. M. Echenique, and Ph. Hofmann, Strong Spin-Orbit Splitting on Bi Surfaces, Phys. Rev. Lett. **93**, 046403 (2004).

[43] T. Hirahara, T. Nagao, I. Matsuda, G. Bihlmayer, E. V. Chulkov, Yu. M. Koroteev, P. M. Echenique, M. Saito, and S. Hasegawa, Role of Spin-Orbit Coupling and Hybridization Effects in the Electronic Structure of Ultrathin Bi Films, Phys. Rev. Lett. **97**, 146803 (2006).

[44] T. Hirahara, K. Miyamoto, I. Matsuda, T. Kadono, A. Kimura, T. Nagao, G. Bihlmayer, E. V. Chulkov, S. Qiao, K. Shimada, H. Namatame, M. Taniguchi, and S. Hasegawa, Direct observation of spin splitting in bismuth surface states, Phys. Rev. B **76**, 153305 (2007).

[45] S. Xiao, D. Wei, and X. Jin, Bi(111) Thin Film with Insulating Interior but Metallic Surfaces, Phys. Rev. Lett. **109**, 166805 (2012).

[46] Z. Chi, G. Qu, Y.-C. Lau, M. Kawaguchi, J. Fujimoto, K. Takanashi, M. Ogata, and M. Hayashi, Spin Hall effect driven by the spin magnetic moment current in Dirac materials, Phys. Rev. B **105**, 214419 (2022).

[47] N. Fukumoto, R. Ohshima, M. Aoki, Y. Fuseya, M. Matsushima, E. Shigematsu, T. Shinjo, Y. Ando, S. Sakamoto, M. Shiga, S. Miwa, M. Shiraishi, Observation of gigantic spin conversion anisotropy in bismuth, arXiv:2208.00589.